Sudden Collapse of Magnetic Order in Oxygen-Deficient Nickelate Films

Jiarui Li,[1] Robert J. Green,[2,3] Zhen Zhang,[4] Ronny Sutarto,[5] Jerzy T. Sadowski,[6] Zhihai Zhu,[1] Grace Zhang,[1] Da Zhou,[1,7] Yifei Sun,[4] Feizhou He,[5] Shriram Ramanathan,[4] and Riccardo Comin[1,*]

[1]*Department of Physics, Massachusetts Institute of Technology, Cambridge, Massachusetts 02139, USA*
[2]*Department of Physics and Engineering Physics, University of Saskatchewan, Saskatoon, Saskatchewan, Canada S7N 5E2*
[3]*Stewart Blusson Quantum Matter Institute, University of British Columbia, Vancouver, British Columbia, Canada V6T 1Z4*
[4]*School of Materials Engineering, Purdue University, West Lafayette, Indiana 47907, USA*
[5]*Canadian Light Source, Saskatoon, Saskatchewan S7N 2V3, Canada*
[6]*Center for Functional Nanomaterials, Brookhaven National Laboratory, Upton, New York 11973, USA*
[7]*School of Physical Science and Technology, ShanghaiTech University, Shanghai 201210, China*

(Received 12 June 2020; revised 17 October 2020; accepted 17 March 2021; published 6 May 2021)

Antiferromagnetic order is a common and robust ground state in the parent (undoped) phase of several strongly correlated electron systems. The progressive weakening of antiferromagnetic correlations upon doping paves the way for a variety of emergent many-electron phenomena including unconventional superconductivity, colossal magnetoresistance, and collective charge-spin-orbital ordering. In this study, we explored the use of oxygen stoichiometry as an alternative pathway to modify the coupled magnetic and electronic ground state in the family of rare earth nickelates ($RENiO_{3-x}$). Using a combination of x-ray spectroscopy and resonant soft x-ray magnetic scattering, we find that, while oxygen vacancies rapidly alter the electronic configuration within the Ni and O orbital manifolds, antiferromagnetic order is remarkably robust to substantial levels of carrier doping, only to suddenly collapse beyond 0.21 e^-/Ni without an accompanying structural transition. Our work demonstrates that ordered magnetism in $RENiO_{3-x}$ is mostly insensitive to carrier doping up to significant levels unseen in other transition-metal oxides. The sudden collapse of ordered magnetism upon oxygen removal may provide a new mechanism for solid-state magnetoionic switching and new applications in antiferromagnetic spintronics.

DOI: 10.1103/PhysRevLett.126.187602

Perovskite-type 3*d* transition-metal oxides (TMOs) realize many interesting electronic phenomena due to their flexibility in accommodating ionic species of varying size and their tolerance to off-stoichiometric chemical compositions. The phase diagrams of these systems host a multitude of broken-symmetry electronic phases, which are often coexisting and intertwined, with long-range antiferromagnetic (AFM) order being a common and stable type of magnetic ground state [1–4]. Oxygen vacancies, whether naturally formed or artificially introduced, provide a very effective avenue to alter the electronic properties of TMOs and in turn suppress, enhance, or engender new emergent phases of matter [3,5–9]. Materials tuning strategies to alter or destabilize an AFM ground state generally proceed via charge compensation doping. The doped carriers can modify the spin state and exchange interaction pathways of transition-metal ions and thus destroy long-range order in systems with strong correlations. Typically, the AFM ordering tendency and transition temperatures are rapidly suppressed upon carrier doping the parent compounds [2–4], setting the stage for new emergent phases to arise.

Rare earth nickelates ($RENiO_3$, RE = Nd, Sm in this study) are a family of TMOs exhibiting a collective organization of the coupled lattice, charge, and spin degrees of freedom that leads to a rich phase diagram [10–13]. Recently, reversible tuning of the oxygen stoichiometry in thin film samples of $RENiO_3$ has been achieved by means of highly controlled post annealing procedures [14,15]. The creation of oxygen vacancies alters the electronic structure via charge compensation, driving the material into a highly insulating state. Oxygen deficiency thus represents a powerful route to tune the electronic and magnetic ground state of $RENiO_{3-x}$, enabling access to their broader electronic and magnetic phase diagram [16–18]. Moreover, recent work on oxygen-reduced $RE_{1-x}Sr_xNiO_2$ has led to the discovery of superconductivity in the nickelate family [19–22], underscoring the importance of studying the ground state properties of oxygen-deficient nickelates.

The high-temperature electronic ground state of stoichiometric $RENiO_3$ is characterized as a negative charge-transfer insulator [23]. The oxygen ligand 2*p* electron is self-doped into the Ni 3*d* orbital leading to a ground state with local electronic configuration $3d^{7+\delta}\underline{L}^{\delta}$, where $\underline{L}$ denotes an oxygen 2*p* hole [24,25]. Upon cooling into the low-temperature insulating phase, a bond and charge disproportionation transition takes place: the NiO_6 octahedra undergo a static, long-range breathing distortion,

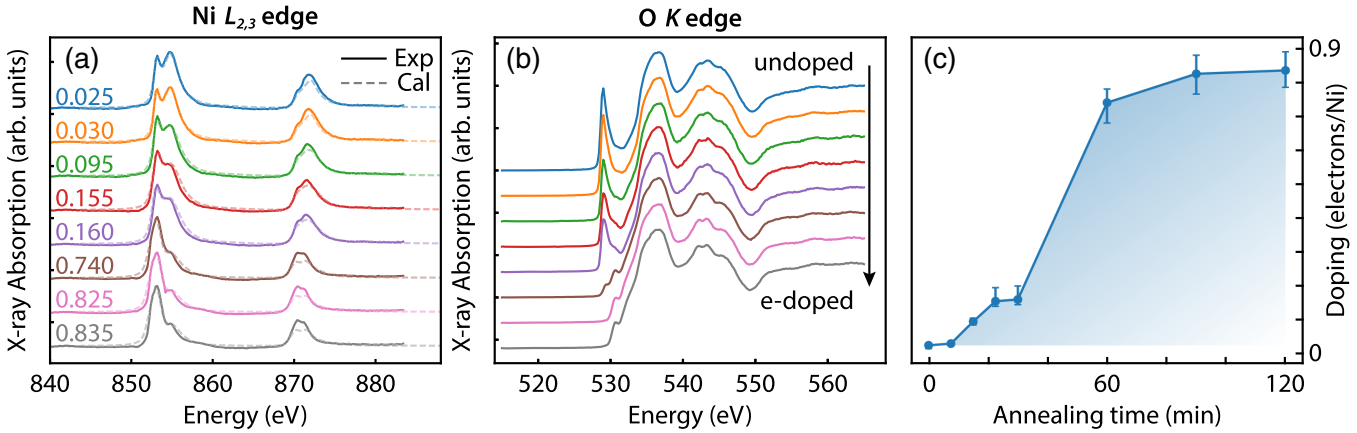

FIG. 1. (a) Measured (solid) and simulated (dashed) x-ray absorption spectra across the Ni $L_{2,3}$ edges for $SmNiO_{3-x}$ with different electron-doping levels, obtained by annealing stoichiometric films in an oxygen deficient atmosphere. The doping level (number of doped electrons per Ni) is specified for each simulated spectrum. Spectra are vertically offset for clarity. (b) x-ray absorption spectra across the O K edges for the same $SmNiO_{3-x}$ samples. The same color legend is used as the data series in Fig. 1(a). (c) The doping levels vs annealing time for each sample, as extracted from the comparison between experimental and theoretical spectra. Vertical error bars reflect the uncertainty in the doping level for each sample.

creating two inequivalent Ni sites. As a result, the electronic degeneracy is further split as

$$2 \times 3d^{7+\delta}\underline{L}^{\delta} \rightarrow 3d^{7+\delta+n_1}\underline{L}^{\delta+n_2} + 3d^{7+\delta-n_1}\underline{L}^{\delta-n_2}, \quad (1)$$

where n_1, n_2 represent the magnitude of the charge and bond disproportionation, respectively. Within the disproportionated phase, magnetic order sets in with a supercell composed of four lattice units along the body diagonal direction of the pseudocubic unit cell and corresponding propagation vector $(1/4, 1/4, 1/4)_{pc}$. Previous studies have found that the spin texture in the AFM phase is either collinear "up-up-down-down" or noncollinear "up-right-down-left" [26–29].

In the present study, we examine the evolution of electronic and magnetic ground state in $RENiO_{3-x}$ using a combination of extended multiplet ligand field theory, x-ray spectroscopy, and resonant soft x-ray scattering. We chart out the electronic and magnetic phase diagram as a function of temperature and oxygen stoichiometry, which reveals the dual role of oxygen vacancies as (electronic) dopants and (magnetic) defects. On the one hand, we find that the removal of oxygens from stoichiometric $RENiO_3$ homogeneously injects electrons into the Ni $3d$ and O $2p$ conduction bands. On the other hand, we observe an unusual evolution of $(1/4, 1/4, 1/4)_{pc}$ magnetic order, which is progressively weakened upon oxygen removal but without a significant change in T_{AFM}, until it collapses at a doping level of $\sim 0.21\ e^-$/Ni. The absence of nanoscale spatial inhomogeneity in the electronic ground state upon doping suggests that the collapse of magnetic order is due to the progressive disruption of the superexchange interaction network caused by the random formation of localized oxygen defect sites with removed O $2p$ ligand orbitals.

To understand how the electronic state in $RENiO_{3-x}$ evolves upon doping, we performed x-ray absorption spectroscopy (XAS) measurements on thin films of $SmNiO_{3-x}$ (SNO) and $NdNiO_{3-x}$ (NNO). More details about the sample and experiment can be found in the Supplemental Material [30]. Figure 1 displays the SNO XAS profiles across the Ni $L_{2,3}$ and O K edges at 22 K, the lowest temperature measured in the present study. At this temperature, both undoped SNO and NNO are well within the insulating state, as signaled by the double peak structure at the Ni L_3 resonance (853.2 and 854.8 eV in Fig. 1(a) and Supplemental Material [30]), which is in close agreement with the literature [25,35]. A sharp and intense prepeak at the O K edge (528.8 eV) corresponds to the transition from O $1s$ core level to the ligand hole $\underline{L}$ in the $3d^{7+\delta}\underline{L}^{\delta}$ configuration [Fig. 1(b)]. Upon doping, we registered the following changes in the XAS spectra: (1) A clear shift of the spectral weight from the high energy to the low energy component in the Ni L_3 XAS profile. The Ni $L_{2,3}$ edge position also shifts to lower energy by about 0.5 eV, from the undoped sample to the highest doping level. In this high doping limit, the XAS spectra are reminiscent of NiO where Ni has a 2+ oxidation state, strongly suggesting that doped carriers have been injected into the Ni conduction band. (2) The prepeak at the O K edge is progressively suppressed until it completely disappears upon doping, indicating that doped carriers reside on the Ni $3d$ orbitals as well as the O ligand band. The disappearance of the XAS prepeak in the highest doping sample suggests the filling of the ligand band upon doping, which resembles the spectra of $LaNiO_{2.5}$ [36]. (3) The NNO spectra manifest a similar trend as SNO. Further details are reported in the Supplemental Material [30].

To elucidate how the doped carriers are distributed in this correlated electronic ground state, we developed an extended multiplet ligand field theory, capable of modeling the ground state properties as well as the XAS of the doped system. Expanding on a previously successful quantum many body double cluster model [31], we have added a

charge reservoir term in the Hamiltonian which can be used to control the electron filling in the model (see Supplemental Material for a complete description of the model [30]). The calculations were implemented using the software QUANTY [37,38]. The simulated SNO XAS spectra are overlaid onto the experimental data in Fig. 1(a) for different doping levels (labeled according to the number of doped electrons per Ni atom). One can see that the simulated spectra capture all of the features and doping trends measured by XAS. By means of a least-squares best-fit analysis of the Ni L_3 XAS edge experimental spectra vs simulated ones, we can infer the doping levels for each sample shown in Fig. 1(a). We note that due to self absorption effects, which extrinsically modulate the relative fluorescence yield at the L_3 and L_2 edges, an approximately 30% discrepancy is found between the simulated and measured data at the Ni L_2 edge [39].

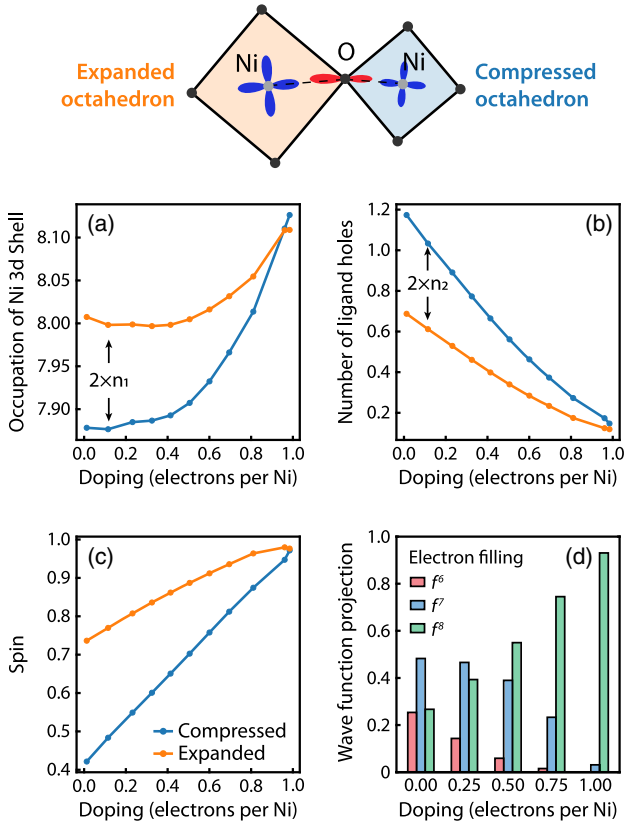

FIG. 2. (top) Double cluster electronic model for $RENiO_3$. The alternating expanded and compressed NiO_6 octahedra, inequivalent Ni $3d$ orbital occupation, and unbalanced O $2p$ orbitals are highlighted. (a)–(c) Doping evolution of the $SmNiO_{3-x}$ electronic structure from double cluster simulation. The evolution of different physical quantities for the two inequivalent sites are shown: (a) occupation of Ni $3d$ orbitals; (b) number of ligand holes; (c) magnitude of Ni spin moments. The charge and bond disproportionation magnitudes as defined in Eq. (1) are marked out by arrows in (a), (b), respectively. (d) The configuration weights of the ground-state wave function decomposed into states with different total electron filling (f^6, f^7, f^8) as a function of doping.

Figure 2 summarizes the effect of electron doping on the SNO electronic structure as captured by the doped double cluster simulation. Upon doping electrons into the system, we expect the extra carriers to redistribute in the oxygen ligand band and Ni $3d$ levels. Figures 2(a) and 2(b) show the occupation of Ni $3d$ orbitals for the two inequivalent Ni sites vs doping. The doped charges mostly occupy the oxygen ligand orbitals, whereas the Ni $3d$ orbitals begin filling only when doping exceeds $\sim 0.5\ e^-$/Ni. The difference in the occupation number between the two sites corresponds to the magnitude of the charge disproportionation (n_1). We note that there is a small amount of charge disproportionation in the undoped SNO sample. The charge disproportionation is found to be initially stable but strongly reduced when doping exceeds 0.5 e^-/Ni. In contrast, the strong bond disproportionation (n_2) presented in the different ligand hole occupation is continuously suppressed to zero upon doping as shown in Fig. 2(b). The doping also gradually changes the spin moments at both Ni sites from low to high spin states [Fig. 2(c)], consistent with previous evidence [14].

The doping-induced carrier redistribution and drastic changes to covalency were investigated by decomposing the ground-state many-electron wave function $|\psi\rangle = \Sigma_{n,i} c_{n,i} |d^{n+i}\underline{L}^i\rangle$ into different Hilbert subspaces f^n (spanned by basis vector $|d^n\underline{L}^0\rangle$, $|d^{n+1}\underline{L}^1\rangle$, $|d^{n+2}\underline{L}^2\rangle \ldots$). The doping evolution of the configuration weight $\Sigma_i c_{n,i}^2$ averaged between compressed and expanded octahedra for sub space f^n where $n = 6, 7, 8$ is shown in Fig. 2(d). The undoped ground-state wave function has significant components in all three subspaces, indicating a highly covalent state. Upon doping, the system drastically loses covalency, and the ground-state wave function is dominated by single f^8 configuration. More details about the decomposition of the ground-state wave function into different basis can be found in Supplemental Material [30].

We then turned our attention to the $(1/4, 1/4, 1/4)_{pc}$ AFM order and its doping dependence. Figure 3(a) shows the rocking curve across the $(1/4, 1/4, 1/4)_{pc}$ magnetic superlattice peak below (solid line) and above (dashed line) the transition temperature for different doping levels and with the incident photon energy tuned at the Ni L_3 resonance (853.2 eV). In the low-doping region ($n < 0.3$), a diffuse magnetic peak is found in all samples at 22 K, gradually decreasing at higher temperatures until it disappears upon warming above the transition temperature. The integrated AFM superlattice peak intensity decreases linearly in the low-doping region [Fig. 3(c)], in contrast to the increase of Ni spin moments obtained from the simulation [Fig. 2(c)]. Despite the suppression of the total scattering intensity, no significant changes in the peak width or shape are observed, suggesting that the suppression of AFM order is not due to the creation of topological defects. The introduction of oxygen vacancies does not alter the thermodynamic properties of the AFM order, as the normalized temperature dependence of the integrated

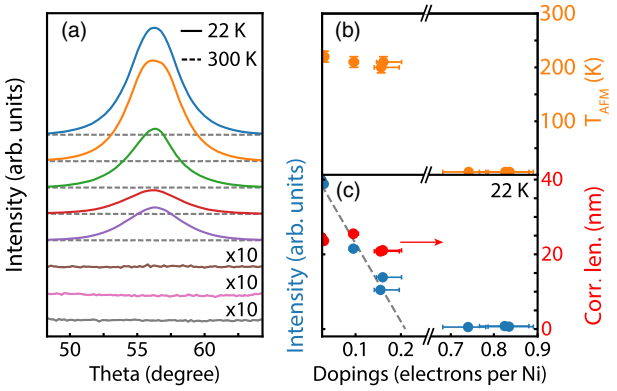

FIG. 3. (a) Rocking curves as a function of sample angle theta, across the $\mathbf{Q}_{\mathrm{AFM}} = (1/4, 1/4, 1/4)_{\mathrm{pc}}$ AFM reflection in $SmNiO_{3-x}$ at 22 K (colored solid line) and 300 K (gray dashed line). The same color legend is used as the XAS data series in Fig. 1. Curves are vertically offset for clarity. The intensity of the last three curves was rescaled to highlight that no scattering signal could be detected above the noise level. (b) Doping dependence of the AFM ordering temperature (T_{AFM}). The T_{AFM} is determined by the temperature when the magnetic peak intensity falls below the noise level. (c) Doping dependence of the magnetic Bragg peak intensity and correlation length measured at 22 K. The dashed line is a linear fit to the data points from samples with AFM order and extrapolates to a threshold doping $n = 0.21$ for the sudden collapse of magnetic order. Note that the vertical error bar is smaller than the marker.

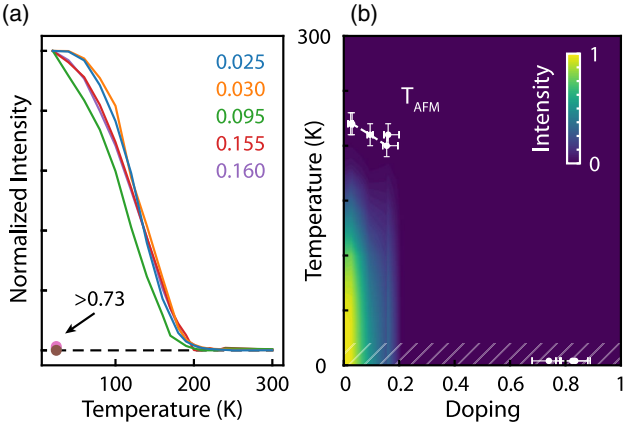

FIG. 4. (a) Temperature dependence of the AFM ordering peak integrated intensity in $SmNiO_{3-x}$. The intensity for the magnetic ordered samples are normalized to the lowest temperature. The same color legend is used as the XAS data series in Fig. 1. (b) Temperature-doping plot of the magnetic phase diagram in $SmNiO_{3-x}$. The magnetic scattering intensity is color coded in the background. The AFM transition temperature for each sample is marked out. The striped area highlights the temperature range that cannot be accessed in our study.

peak intensity are highly overlapped for the first five doping levels [Fig. 4(a)]. No magnetic scattering intensity was observed above the noise level for higher doping levels ($n > 0.6$) and down to 22 K, the lowest temperature measured in the present study. We note that the suppression of the $(1/4, 1/4, 1/4)_{\mathrm{pc}}$ AFM order does not preclude the emergence of magnetic order with different ordering vectors as previously found in the oxygen-reduced nickelates [9,40,41].

The temperature-doping phase diagram is sketched out in Fig. 4(b). The $(1/4, 1/4, 1/4)_{\mathrm{pc}}$ magnetic order is suppressed upon doping and collapses beyond a doping level of ~0.21, as determined by a linear extrapolation of the intensity-doping scaling for the low-doping samples, while the AFM transition temperature remains almost unchanged.

Oxygen vacancies are known to suppress the magnetic ordering temperature in manganites and cobaltites [42–44], or give rise to new magnetic phases through ordering of oxygen defects [45,46]. However, a reduction of the magnetic order parameter with no significant variation in the ordering temperature is unreported. A few scenarios are examined to explain the simultaneous increase of the Ni spin moment and decrease of the AFM order parameter, while T_{AFM} remains unchanged. First, a microscopic phase separation picture may be invoked to explain the experimental results: the inhomogeneous distribution of oxygen vacancies creates two phases, with undoped AFM regions coexisting alongside doped nonmagnetic ones. Upon doping, the AFM scattering intensity decreases linearly as the coverage of undoped regions is reduced, while the T_{AFM} remains unchanged. To assess this possibility, we have performed a spectromicroscopy study using x-ray photoemission electron microscopy (XPEEM). No systematic electronic inhomogeneity was observed at either the O K edge or Ni L edge, down to the length scale of our spatial resolution limit (~10 nm), indicating a homogeneous electronic state with spatially uniform carrier doping. Details of the XPEEM data are described in the Supplemental Material [30].

With a phase segregation scenario ruled out, we focused on an atomistic picture to explain the phase diagram. In this picture, the superexchange interaction between neighboring Ni spins is mediated by oxygen ligands. Each Ni atom is linked to its six nearest-neighbor Ni sites via six octahedrally coordinated oxygen atoms. The removal of oxygen not only alters the local Ni charges and spin moments via an effective doping mechanism, but it also destroys the superexchange interaction pathways that mediate the magnetic interaction across Ni moments. When the density of oxygen vacancies is low, long-range AFM order can still be sustained. When the atomic-scale disruption of the 3D magnetic superexchange network reaches a given threshold, long-range magnetic order can no longer be supported. In our study, AFM order disappears at a doping level of around 0.21 electrons/Ni, corresponding to $SmNiO_{2.90}$.

In summary, we have systematically studied the electronic and magnetic structure of $RENiO_{3-x}$ (Re = Sm, Nd).

The introduction of oxygen vacancies is shown to be an effective approach to continuously tune the $3d^{7+\delta}\underline{L}^{\delta}$ electronic ground state. We also show that electron doping has only marginal effect on $(1/4, 1/4, 1/4)_{pc}$ AFM order except for a suppression of the ordering strength. The magnetic order collapses around a doping threshold of $n \sim 0.21$.

The AFM ground state is vulnerable to carrier doping due to the nature of the superexchange interaction [47]. Indeed, in systems with strong correlations, there is a consensus that the AFM order is fragile and rapidly suppressed to $T = 0$ K upon electron or hole doping, as unveiled in the family of cuprates, manganites, iron pnictides, among others [2–4]. Our study reveals a new kind of AFM order that is mostly insensitive to carrier doping, and a notable exception to the established phenomenology of other correlated electron systems. At the same time, the sharp erasure of magnetic order that is uniquely enabled by oxygen removal in rare earth nickelates creates interesting new possibilities for use of reversible magnetoionic switching in antiferromagnetic spintronic devices, low-power logic devices, and nonvolatile memory cells [48].

We wish to thank Alex McLeod, William Zheng, George A. Sawatzky, Bernhard Keimer, Eva Benckiser, Matthias Hepting, Alex Fraño, and John Mitchell for insightful discussions. This work was supported by the Air Force Office of Scientific Research Young Investigator Program under Grant No. FA9550-19-1-0063. Part of this research was supported by the National Science Foundation under Grant No. 1751739. R. J. G. was supported by the Natural Sciences and Engineering Research Council of Canada (NSERC). Part of the research described in this Letter was performed at the Canadian Light Source, a national research facility of the University of Saskatchewan, which is supported by the Canada Foundation for Innovation (CFI), NSERC, the National Research Council (NRC), the Canadian Institutes of Health Research (CIHR), the Government of Saskatchewan, and the University of Saskatchewan. This research used resources of the Center for Functional Nanomaterials and National Synchrotron Light Source II, which are U.S. Department of Energy Office of Science Facilities at Brookhaven National Laboratory under Contract No. DE-SC0012704. S. R. acknowledges AFOSR Grant No. FA9550-19-1-0351 for support.

*rcomin@mit.edu

[1] E. Fradkin, S. A. Kivelson, and J. M. Tranquada, Theory of intertwined orders in high temperature superconductors, Rev. Mod. Phys. **87**, 457 (2015).

[2] E. Dagotto, Complexity in strongly correlated electronic systems, Science **309**, 257 (2005).

[3] B. Keimer, S. A. Kivelson, M. R. Norman, S. Uchida, and J. Zaanen, From quantum matter to high-temperature superconductivity in copper oxides, Nature (London) **518**, 179 (2015).

[4] P. Dai, Antiferromagnetic order and spin dynamics in iron-based superconductors, Rev. Mod. Phys. **87**, 855 (2015).

[5] J. L. Tallon, Oxygen in high-T_c cuprate superconductors, in *Frontiers in Superconducting Materials* (Springer-Verlag, Berlin/Heidelberg, 2005), pp. 295–330, https://doi.org/10.1007/3-540-27294-1_7.

[6] M. M. Seikh, C. Simon, V. Caignaert, V. Pralong, M. B. Lepetit, S. Boudin, and B. Raveau, New magnetic transitions in the ordered oxygen-deficient perovskite $LnBaCo_2O_{5.50+\delta}$, Chem. Mater. **20**, 231 (2008).

[7] G. Herranz, M. Basletic, M. Bibes, C. Carrétéro, E. Tafra, E. Jacquet, K. Bouzehouane, C. Deranlot, A. Hamzić, J.-M. Broto, A. Barthélémy, and A. Fert, High Mobility in $LaAlO_3/SrTiO_3$ Heterostructures: Origin, Dimensionality, and Perspectives, Phys. Rev. Lett. **98**, 216803 (2007).

[8] Z. Zeng, M. Greenblatt, and M. Croft, Large magnetoresistance in antiferromagnetic $CaMnO_{3-\delta}$, Phys. Rev. B **59**, 8784 (1999).

[9] R. D. Sánchez, M. T. Causa, A. Caneiro, A. Butera, M. Vallet-Regí, M. J. Sayagués, J. González-Calbet, F. García-Sanz, and J. Rivas, Metal-insulator transition in oxygen-deficient $LaNiO_{3-x}$ perovskites, Phys. Rev. B **54**, 16574 (1996).

[10] J. B. Torrance, P. Lacorre, A. I. Nazzal, E. J. Ansaldo, and C. Niedermayer, Systematic study of insulator-metal transitions in perovskites $RNiO_3$ (R = Pr, Nd, Sm, Eu) due to closing of charge-transfer gap, Phys. Rev. B **45**, 8209 (1992).

[11] G. Catalan, Progress in perovskite nickelate research, Phase Transitions **81**, 729 (2008).

[12] S. Middey, J. Chakhalian, P. Mahadevan, J. Freeland, A. Millis, and D. Sarma, Physics of ultrathin films and heterostructures of rare-earth nickelates, Annu. Rev. Mater. Res. **46**, 305 (2016).

[13] S. Catalano, M. Gibert, J. Fowlie, J. Íñiguez, J.-M. Triscone, and J. Kreisel, Rare-earth nickelates $RNiO_3$: thin films and heterostructures, Rep. Prog. Phys. **81**, 046501 (2018).

[14] L. Wang, S. Dash, L. Chang, L. You, Y. Feng, X. He, K. J. Jin, Y. Zhou, H. G. Ong, P. Ren, S. Wang, L. Chen, and J. Wang, Oxygen vacancy induced room-temperature metal–insulator transition in nickelate films and its potential application in photovoltaics, ACS Appl. Mater. Interfaces **8**, 9769 (2016).

[15] M. Kotiuga, Z. Zhang, J. Li, F. Rodolakis, H. Zhou, R. Sutarto, F. He, Q. Wang, Y. Sun, Y. Wang, N. A. Aghamiri, S. B. Hancock, L. P. Rokhinson, D. P. Landau, Y. Abate, J. W. Freeland, R. Comin, S. Ramanathan, and K. M. Rabe, Carrier localization in perovskite nickelates from oxygen vacancies, Proc. Natl. Acad. Sci. U.S.A. **116**, 21992 (2019).

[16] I. V. Nikulin, M. A. Novojilov, A. R. Kaul, S. N. Mudretsova, and S. V. Kondrashov, Oxygen nonstoichiometry of $NdNiO_{3-\delta}$ and $SmNiO_{3-\delta}$, Mater. Res. Bull. **39**, 775 (2004).

[17] A. Tiwari and K. Rajeev, Effect of oxygen stoichiometry on the electrical resistivity behaviour of $NdNiO_{3-\delta}$, Solid State Commun. **109**, 119 (1998).

[18] J. L. García-Muñoz, M. Suaaidi, M. J. Martínez-Lope, and J. A. Alonso, Influence of carrier injection on the

metal-insulator transition in electron- and hole-doped $R_{1-x}A_xNiO_3$ perovskites, Phys. Rev. B **52**, 13563 (1995).
[19] D. Li, K. Lee, B. Y. Wang, M. Osada, S. Crossley, H. R. Lee, Y. Cui, Y. Hikita, and H. Y. Hwang, Superconductivity in an infinite-layer nickelate, Nature (London) **572**, 624 (2019).
[20] D. Li, B. Y. Wang, K. Lee, S. P. Harvey, M. Osada, B. H. Goodge, L. F. Kourkoutis, and H. Y. Hwang, Superconducting Dome in $Nd_{1-x}Sr_xNiO_2$ Infinite Layer Films, Phys. Rev. Lett. **125**, 027001 (2020).
[21] S. Zeng, C. S. Tang, X. Yin, C. Li, M. Li, Z. Huang, J. Hu, W. Liu, G. J. Omar, H. Jani, Z. S. Lim, K. Han, D. Wan, P. Yang, S. J. Pennycook, A. T. S. Wee, and A. Ariando, Phase Diagram and Superconducting Dome of Infinite-Layer $Nd_{1-x}Sr_xNiO_2$ Thin Films, Phys. Rev. Lett. **125**, 147003 (2020).
[22] M. Osada, B. Y. Wang, K. Lee, D. Li, and H. Y. Hwang, Phase diagram of infinite layer praseodymium nickelate $Pr_{1-x}Sr_xNiO_2$ thin films, Phys. Rev. Mater. **4**, 121801(R) (2020).
[23] J. Zaanen, G. A. Sawatzky, and J. W. Allen, Band Gaps and Electronic Structure of Transition-Metal Compounds, Phys. Rev. Lett. **55**, 418 (1985).
[24] T. Mizokawa, D. I. Khomskii, and G. A. Sawatzky, Spin and charge ordering in self-doped Mott insulators, Phys. Rev. B **61**, 11263 (2000).
[25] V. Bisogni, S. Catalano, R. J. Green, M. Gibert, R. Scherwitzl, Y. Huang, V. N. Strocov, P. Zubko, S. Balandeh, J.-M. Triscone, G. Sawatzky, and T. Schmitt, Ground-state oxygen holes and the metal–insulator transition in the negative charge-transfer rare-earth nickelates, Nat. Commun. **7**, 13017 (2016).
[26] J. L. García-Muñoz, J. Rodríguez-Carvajal, and P. Lacorre, Sudden appearance of an unusual spin density wave at the metal-insulator transition in the perovskites $RNiO_3$(R =Pr, Nd), Europhys. Lett. **20**, 241 (1992).
[27] V. Scagnoli, U. Staub, A. M. Mulders, M. Janousch, G. I. Meijer, G. Hammerl, J. M. Tonnerre, and N. Stojic, Role of magnetic and orbital ordering at the metal-insulator transition in $NdNiO_3$, Phys. Rev. B **73**, 100409(R) (2006).
[28] A. Frano, E. Schierle, M. W. Haverkort, Y. Lu, M. Wu, S. Blanco-Canosa, U. Nwankwo, A. V. Boris, P. Wochner, G. Cristiani, H. U. Habermeier, G. Logvenov, V. Hinkov, E. Benckiser, E. Weschke, and B. Keimer, Orbital Control of Noncollinear Magnetic Order in Nickel Oxide Heterostructures, Phys. Rev. Lett. **111**, 106804 (2013).
[29] M. Hepting *et al.*, Complex magnetic order in nickelate slabs, Nat. Phys. **14**, 1097 (2018).
[30] See Supplemental Material at http://link.aps.org/supplemental/10.1103/PhysRevLett.126.187602 for additional details, which includes Refs. [15,31–34].
[31] R. J. Green, M. W. Haverkort, and G. A. Sawatzky, Bond disproportionation and dynamical charge fluctuations in the perovskite rare-earth nickelates, Phys. Rev. B **94**, 195127 (2016).
[32] M. Medarde, A. Fontaine, J. L. García-Muñoz, J. Rodríguez-Carvajal, M. De Santis, M. Sacchi, G. Rossi, and P. Lacorre, $RNiO_3$ perovskites (R = Pr, Nd): Nickel valence and the metal-insulator transition investigated by x-ray-absorption spectroscopy, Phys. Rev. B **46**, 14975 (1992).
[33] M. W. Haverkort, Spin and orbital degrees of freedom in transition metal oxides and oxide thin films studied by soft x-ray absorption spectroscopy, Ph. D. thesis, University of Koln, 2005.
[34] J. C. Slater and G. F. Koster, Simplified LCAO method for the periodic potential problem, Phys. Rev. **94**, 1498 (1954).
[35] F. Y. Bruno, S. Valencia, R. Abrudan, Y. Dumont, C. Carrtro, M. Bibes, and A. Barthélémy, Probing the metal-insulator transition in nickelates using soft x-ray absorption spectroscopy, Appl. Phys. Lett. **104**, 021920 (2014).
[36] M. Abbate, G. Zampieri, F. Prado, A. Caneiro, J. M. Gonzalez-Calbet, and M. Vallet-Regi, Electronic structure and metal-insulator transition in $LaNiO_{3-\delta}$, Phys. Rev. B **65**, 155101 (2002).
[37] M. W. Haverkort, M. Zwierzycki, and O. K. Andersen, Multiplet ligand-field theory using Wannier orbitals, Phys. Rev. B **85**, 165113 (2012).
[38] M. W. Haverkort, Quanty for core level spectroscopy - excitons, resonances and band excitations in time and frequency domain, J. Phys. **712**, 012001 (2016).
[39] S. Eisebitt, T. Böske, J.-E. Rubensson, and W. Eberhardt, Determination of absorption coefficients for concentrated samples by fluorescence detection, Phys. Rev. B **47**, 14103 (1993).
[40] T. Moriga, O. Usaka, I. Nakabayashi, Y. Hirashima, T. Kohno, S. Kikkawa, and F. Kanamaru, Reduction of the perovskite-type $LnNiO_3$ (Ln = Pr, Nd) to $Ln_3Ni_3O_7$ with monovalent nickel ions, Solid State Ionics **74**, 211 (1994).
[41] J. A. Alonso, M. J. Martínez-Lope, J. L. García-Muñoz, and M. T. Fernández-Díaz, A structural and magnetic study of the defect perovskite $LaNiO_{2.5}$ from high-resolution neutron diffraction data, J. Phys. Condens. Matter **9**, 6417 (1997).
[42] S. V. Trukhanov, I. O. Troyanchuk, N. V. Pushkarev, and H. Szymczak, The influence of oxygen deficiency on the magnetic and electric properties of $La_{0.70}Ba_{0.30}MnO_{3-\delta}$($0 \leq \delta \leq 0.30$) manganite with a perovskite structure, J. Exp. Theor. Phys. **95**, 308 (2002).
[43] W. Zhong, H. Y. Jiang, X. L. Wu, N. J. Tang, W. Chen, and Y. W. Du, Magnetic and transport properties of oxygen-deficient perovskite manganites, Chin. Phys. Lett. **20**, 742 (2003).
[44] S. Balamurugan, K. Yamaura, A. B. Karki, D. P. Young, M. Arai, and E. Takayama-Muromachi, Specific-heat evidence of strong electron correlations and thermoelectric properties of the ferromagnetic perovskite $SrCoO_{3-\delta}$, Phys. Rev. B **74**, 172406 (2006).
[45] F. Ramezanipour, J. E. Greedan, J. Siewenie, R. L. Donaberger, S. Turner, and G. A. Botton, A vacancy-disordered, oxygen-deficient perovskite with long-range magnetic ordering: local and average structures and magnetic properties of $Sr_2Fe_{1.5}Cr_{0.5}O_5$, Inorg. Chem. **51**, 2638 (2012).
[46] B.-X. Wang, S. Rosenkranz, X. Rui, J. Zhang, F. Ye, H. Zheng, R. F. Klie, J. F. Mitchell, and D. Phelan, Antiferromagnetic defect structure in $LaNiO_{3-\delta}$ single crystals, Phys. Rev. Mater. **2**, 064404 (2018).
[47] J. B. Goodenough, *Magnetism and the Chemical Bond* (Interscience, New York, 1963).
[48] T. Jungwirth, X. Marti, P. Wadley, and J. Wunderlich, Antiferromagnetic spintronics, Nat. Nanotechnol. **11**, 231 (2016).